# Viscosity of fluid membranes measured from vesicle deformation

Hammad A. Faizi[a], Rumiana Dimova[b], Petia M. Vlahovska[ac]
[a] *Department of Mechanical Engineering, McCormick School of Engineering and Applied Science, Northwestern University, Evanston, IL 60208, USA* [b] *Max Planck Institute of Colloids and Interfaces, Science Park Golm, 14424 Potsdam, Germany* [c] *Department of Engineering Sciences and Applied Mathematics, McCormick School of Engineering and Applied Science, Northwestern University, Evanston, IL 60208, USA, E-mail: petia.vlahovska@northwestern.edu*
(Dated: March 4, 2021)

Viscosity is a key mechanical property of cell membranes that controls time-dependent processes such as membrane deformation and diffusion of embedded inclusions. Despite its importance, membrane viscosity remains poorly characterized because existing methods rely on complex experimental designs and/or analyses. Here, we describe a facile method to determine the viscosity of bilayer membranes from the transient deformation of giant unilamellar vesicles induced by a uniform electric field. The method is non-invasive, easy to implement, probe-independent, high-throughput, and sensitive enough to discern membrane viscosity of different lipid types, lipid phases, and polymers in a wide range, from $10^{-8}$ to $10^{-4}$ Pa.s.m. It enables fast and consistent collection of data that will advance understanding of biomembrane dynamics.

Cells and cellular organelles are enveloped by membranes composed primarily of lipid bilayers. The lipid bilayer is held together by non-covalent bonds, which allow for the lipid molecules to rearrange freely. As a result, the membrane behaves as a viscous fluid [1]. Membrane fluidity impacts membrane-dependent functions [2, 3], however, its quantification has remained elusive. Viscosity is the common measure for fluidity, yet for membranes this property has been difficult to assess. Existing experimental methods rely on estimates from the diffusion coefficients of domains [4–6] or membrane-anchored nanoparticles [7], analysis of domain shape fluctuations [8], bilayer thickness fluctuations measured with neutron spin echo spectroscopy [9], or fluorescence lifetime imaging of small synthetic molecules called "molecular rotors" [10]. Application of mechanical stress has also been utilized to measure membrane viscosity, for example, from the rate of tether formation [11] or the flow pattern on giant vesicles driven by applied shear flow [12] or point-force [13]. These methods require either complex equipment or analyses, which makes most of them low through-put and not easy to implement. Furthermore, values obtained by different approaches vary greatly. Despite significant effort, membrane viscosity remains poorly characterized and there is a need for a facile method to measure it in a consistent manner.

In this study, we show how vesicle electrodeformation, previously used to measure bending rigidity of membranes [14–16], can be employed to obtain membrane viscosity. Upon application of a uniform AC electric field, a quasi-spherical vesicle deforms into a prolate ellipsoid. The aspect ratio increases and reaches steady state. When the field is switched off the vesicle relaxes back to its equilibrium spherical shape, see Fig. 1 and Movie S1 in the Supporting Information (SI). The rate at which the vesicle elongates while the field is on, and relaxes back to its equilibrium shape after the field is turned off, is directly related to the membrane viscosity [17, 18].

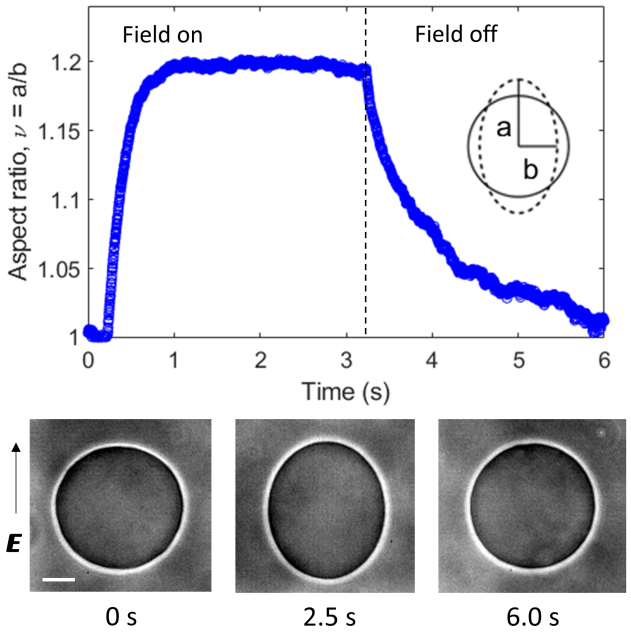


FIG. 1. Top: Prolate deformation of a POPC giant vesicle in an uniform electric field with amplitude $E_0$=10 kV/m and frequency of 1 kHz. Bottom: Snapshots of the vesicle during the experiment. Imaging with phase contrast microscopy. Scale bar: 7.5 $\mu$m.

We adapt the theory developed in [17, 19–22] to account for membrane viscosity (see SI Section III) and describe the observed vesicle deformation upon application of the field

$$\nu(t) = 1 + \frac{9\varepsilon E_0^2 R}{64\sigma}\left(1 - \exp\left(-\frac{24\sigma}{\eta R\,(55 + 16\chi_m)}t\right)\right) \tag{1}$$

where $\chi_m = \eta_m/\eta R$ is the dimensionless membrane viscosity $\eta_m$, $\sigma$ is the membrane tension in the presence of

electric field, $R$ is the vesicle radius, $E_0$ is the amplitude of the applied field, $\eta$ is the viscosity, and $\varepsilon$ is the permittivity of the solution inside and outside the vesicle (assumed to be the same). Expanding the exponential in Eq. 13 in Taylor series shows that initially the aspect ratio increases linearly with time

$$\nu = 1 + \frac{t}{t_{\rm ed}} \left( \frac{27}{8\,(55 + 16\chi_m)} \right) \qquad (2)$$

where $1/t_{\rm ed} = \varepsilon E_0^2/\eta$ is the characteristic scale for the rate of electrodeformation. Thus, the membrane viscosity can be obtained from the slope of the $\nu(t)$ curve immediately after the application of the field.

To test this hypothesis, we prepared giant unilamellar vesicles (GUVs) with various membrane compositions (see SI Section I for details about the methods of preparation, imaging and the electrodeformation set-up). Indeed, the elongation curves of the same GUV at differen1 kHzt field strengths show linear increase, see Fig. 2. Fitting the slope to Eq. 2 yields the membrane viscosity.

The linear response occurs only if the restoring force of the membrane tension is negligible compared to the deforming electric stress. This corresponds to time $t \ll \eta R/\sigma$, which is in the order of 1-10 s for typical values of $\sigma = 10^{-9} - 10^{-8}$ N/m, $\eta = 10^{-3}$ Pa.s and $R = 10\,\mu$m. The low tension of vesicles makes this linear regime possible. If the tension is high, one needs to fit the entire curve including the plateau; this situation arises when applying the method to drops (see SI Section IV).

The time limit for the linear approximation can be estimated by comparing the linear and quadratic terms in the Taylor series of the exponential term in Eq. 13. The two terms become equal if $t/t_{\rm ed} = (55 + 16\chi_m)\varepsilon E_0^2/12\sigma$. Considering typical parameters $\varepsilon E_0^2/\sigma \sim 1$, yields $t/t_{\rm ed} \sim 5$ if $\chi_m \sim 0$. Higher membrane viscosity extends the linear deformation regime, if $\chi_m \sim 10$, as in polymersomes made of $PBd_{22}$-*b*-$PEO_{14}$, where the cut-off time becomes $t/t_{\rm ed} \sim 15$, see Fig. 3.

To use Equation Eq. 2 in experiments it is important that (i) the membrane capacitor is fully charged, and (ii) the membrane capacitor remains fully charged while the vesicle is deforming. The first condition is met if the field frequency $\omega \ll \omega_c \sim \lambda/RC_m$. Typically, the bulk solution conductivity $\lambda \sim 10^{-3}$ S/m, the membrane capacitance $C_m \sim 0.01$ F/m$^2$, thus a good choice for the working frequency is less than 10 kHz. The second condition requires that the time over which the vesicle deforms, $t_{\rm ed}$, is longer than the capacitor charging time, $t_m \sim \omega_c^{-1}$. Since $\omega_c \sim 10$ kHz, the capacitor charges or discharges much faster (on a sub-ms time scale) compared to the deformation time scale ($\sim 0.1$ second). Another consideration in the design of the experiment is the electric field amplitude. It should not be too high in order to avoid membrane poration and to ensure that

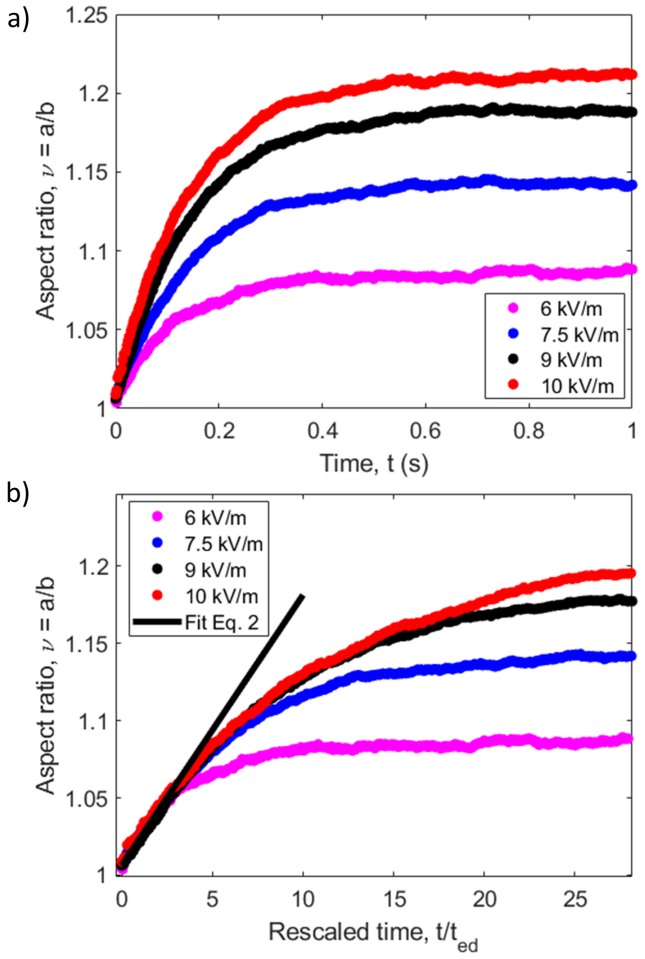


FIG. 2. Deformation of a giant vesicle in an applied uniform electric field (at 1 kHz). (a) A POPC vesicle ($R$ =30.1 $\mu m$) exposed to fields of different amplitude. (b) The initial slope of the data in (a) replotted as a function of the rescaled time $t/t_{\rm ed}$ yields for the viscosity $\eta_m = 2.63 \pm 0.41 \times 10^{-7}$ Pa.s.m.

vesicle deformation remains small so that the theoretical model applies. The electroporation limit is estimated from $E_c = 2\,V_c/3R$. The critical poration voltage, $V_c$, for a lipid membrane is approximately 1 V, corresponding to field strength of about 100 kV/m for a vesicle with radius $R = 10\,\mu$m [23, 24]; for polymer membranes the poration limit is higher $V_c \sim$ 4-8 V [25, 26]. Small deformation is ensured if the electric field stresses are weaker than the tension and bending forces that are keeping the vesicle quasi-spherical, i.e., $\varepsilon E_0^2 R/\sigma < 1$. For a vesicle with radius $R = 10\,\mu$m and tension $\sigma = 10^{-8}$ N/m this requires that $E_0 \leq 10$ kV/m.

Eq. 2 shows that the method is sensitive to the membrane viscosity only if the term $16\chi_m$ is comparable or larger than 55. This requires $\eta_m/\eta R \geq 1$, i.e., the Saffmann-Delbruck's length exceeding the vesicle radius. Thus, if the vesicle radius is 10 $\mu$m, only membrane viscosity above $10^{-8}$ Pa.s.m could be detected. The higher $\eta_m/\eta R$, the more accurate the method is. This condi-

tion is easily satisfied in polymersomes, which makes our method particularly suitable for measurement of the viscosity of polymer membranes, for which data are scarce.

We tested our method with GUVs membranes composed of palmitoyloleoylphosphatidylcholine (POPC), dioleoylphosphatidylcholine (DOPC), cholesterol (Chol), dimyristoylphosphatidylcholine (DMPC), stearoyloleoylphosphatidylcholine (SOPC), dipalmitoylphosphatidylcholine (DPPC) and poly(butadiene)-*b*-poly(ethylene oxide) diblock copolymers, $PBd_x$-*b*-$PEO_y$. The same vesicle was subjected to field with increasing strength ranging from 4-10 kV/m. The applied frequency was kept as 0.5-1 kHz. We recorded the vesicle fluctuations for fluctuation spectroscopy [15, 27, 28] to determine the equilibrium membrane tension and bending rigidity before and after the electric field application, see SI Section I. No changes were detected due to the exposure to the electric field. The same procedure was repeated again at least 3-4 times for the same vesicle. The method reproducibility for the same vesicle is discussed in SI Section III. The error reported for every vesicle composition is determined by computing the standard deviation over the vesicle population (typically 20 vesicles).

TABLE I. Measured membrane viscosities for different phospholipids and a polymer at temperature 25.0°C, see also SI Table S1. The values in brackets indicate tail unsaturation (first column) and the number of measured vesicles per composition (last column).

| Composition | $\eta_m$ [$10^{-8}$ Pa.s.m] |
|---|---|
| DOPC (18:1) | 6.4 ±3.4 (19) |
| POPC (16:0-18:1) | 23.4 ±11.1 (21) |
| SOPC (18:0-18:1) | 21.4 ±4.0 (20) |
| DMPC (14:0) | 48.0 ±15.8 (17) |
| $PBd_{22}$-*b*-$PEO_{14}$ | 55.7 ±7.0 (22) |

Viscosities of different types of single component membranes are listed in Table I. The block copolymer $PBd_{22}$-*b*-$PEO_{14}$ has the highest viscosity as expected from its longer (compared to a lipid) chain. The molecular weight $M_w$ of the lipids used in experiments is approximately 700-800 g/mol while $PBd_{22}$-*b*-$PEO_{14}$ has $M_w$ = 1350 g/mol. Among the lipids, the viscosity decreases with the number of unsaturated bonds in the hydrophobic tail. DMPC exhibits the highest viscosity, followed by POPC, SOPC and DOPC. DMPC, POPC and DOPC have none, one and two unsaturated bond in their hydrophobic tails, respectively. Note that DMPC is very close to its main phase transition of 24.0°C. Our results show a good order of magnitude agreement with other macroscopic approaches like falling ball viscosimetry, optical dynamometry, shear rheometry and probe diffusion methods [7, 29–31].

The membrane viscosity of these single-component bilayers also correlates with the area per lipid head where

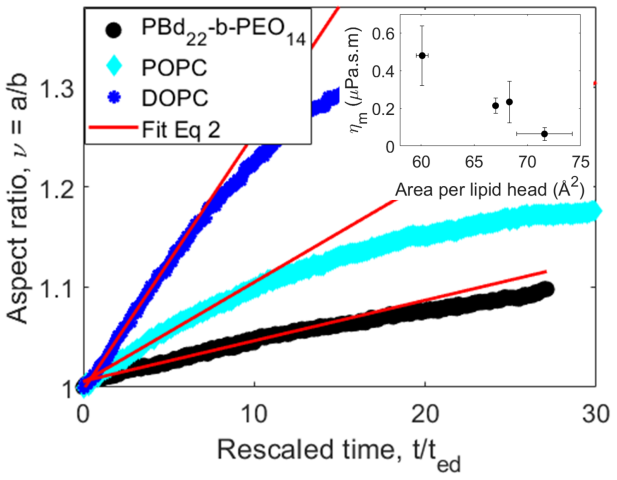


FIG. 3. Transient electrodeformation of DOPC, POPC and $PBD_{22}PEO_{14}$. The field strength for DOPC and POPC is 10 kV/m while for $PBd_{22}$-*b*-$PEO_{14}$ is 8 kV/m (1 kHz). The solid line represents the theoretical fit with Eq. 2. The inset shows the dependence of membrane viscosity on area per lipid headgroup. The error in area per lipid head reflects the range of values measured by different research groups, see Table S1 in the SI for details.

the viscosity decreases, see inset of Fig. 3. This is reasonable considering that smaller area per lipid head would lead to tighter packing thereby offering stronger Van der Waal interactions between lipid tails and higher resistance to lipid flows [32].

TABLE II. Measured membrane viscosities for DOPC:DPPC:Chol ternary system at temperature, 25.0°C. $L_d$, $L_o$ and $S_o$ represent liquid disordered, liquid ordered and solid phases respectively. The values in brackets indicate lipid molar ratios (first column) and the number of measured vesicles per composition (last column).

| Composition | Phase | $\eta_m$ [$10^{-8}$ Pa.s.m] |
|---|---|---|
| DOPC | $L_d$ | 6.4 ±3.4 (19) |
| DOPC:Chol (1:1) | $L_d$ | 20.5 ±13.0 (25) |
| DOPC:DPPC (1:1) | $L_d + S_o$ | 15.3 ±6.5 (20) |
| DOPC:DPPC:Chol (2:1:1) | $L_d + L_o$ | 22.0 ±13.0 (22) |
| DPPC:Chol (1:1) | $L_o$ | 32.3 ±12.4 (25) |
| DOPC:DPPC:Chol (1:1:1) | $L_d + L_o$ | 12.6 ±4.6 (18) |
| DOPC:DPPC:Chol (1:1:2) | $L_o$ | 20.7 ±12.6 (25) |

Next, we applied our method to measure the viscosity of DOPC:DPPC:Chol bilayers. Phase separation was detected using the fluorescent marker, Liss Rhod PE (0.1 % mole fraction). Imaging with confocal microscopy showed that pure DOPC, 1:1 DOPC:Chol, 1:1 DPPC:Chol, 1:1:1 DOPC:DPPC:Chol, 1:1:2 DOPC:DPPC:Chol exhibited homogeneous fluorescence. 1:1 DOPC:DPPC demonstrated phase separation with intricate network of finger-like domains indicative of gel or solid phase with liquid disordered state at equilibrium. For 2:1:1

DOPC:DPPC:Chol, we observed 1-2 $\mu$m circular domains, see SI Fig. S1. Table II lists the membrane viscosities obtained with our electrodeformation method. Pure DOPC exhibits the lowest viscosity. Adding DPPC or/and cholesterol increases the viscosity, and the effect of the cholesterol is more pronounced. The modest increase in viscosity for the DOPC:DPPC phase separated mixture could be estimated from the viscosity of a 2D suspension, $\eta_{eff} = \eta_{DOPC}(1 + 2\phi)$, where $\phi \sim 0.4$ is the fraction of the solid phase [33]. However, the more significant effect of Chol is likely due to increased packing [34]. We have compared our results with measurements of the diffusion constant [35] in this ternary system, also see SI Table S2. In general, increasing viscosity correlates with decreasing diffusivity, however, it is not trivial to directly correlate the values of the diffusion constant and membrane viscosity.

We also compare our results with methods that have directly obtained the membrane viscosity. *Cicuta et al.* measured the membrane viscosity for mixed DOPC:DPPC:Chol in the range 0.1-5$\times 10^{-7}$ Pa.s.m from diffusion of lipid domains [4] with a good order of magnitude match for our system. Shear rheological methods have also obtained values ranging $10^{-8}$-$10^{-6}$ Pa.s.m for liquid ordered systems [36] and point-force methods have obtained a value ranging $10^{-9}$-$10^{-6}$ Pa.s.m [13].

There is scarcity of membrane viscosity data for polymersomes. To our best knowledge, the only direct shear viscosity measurements can be found in *Dimova et al* [37] for $PBd_{33}$-*b*-$PEO_{20}$. Here, we have explored a library of diblock copolymers, $PBd_x$-*b*-$PEO_y$, for varying molecular weight, $M_w$, from 0.7 kDa to 6.8 kDa as shown in Fig. 4. Interestingly, around 1.8 kDa polymer membranes exhibit a significant increase in the shear membrane viscosity (note that the data are plotted in logarithmic scale). This suggests the possibility of chain entanglements for higher $M_w$ polymersomes [38], reducing the overall mobility significantly. Our results are in agreement with the abrupt change in diffusivity previously observed by *Srinivas et al.* [39]. Higher $M_w$ polymersomes also have a thicker hydrophobic core resulting in a larger bending rigidity compared to phospholipids [40]. The inset of Fig. 4 shows that the bending rigidity follows a power-law dependence on $M_w$. The exponent is consistent with the power-law dependence of membrane thickness on the molecular weight $h \sim M_w^n$, where $n$ lies within the theoretical bounds of 0.5 (random Gaussian coil) and 1 (full stretch). Given that $\kappa \sim h^2$, it follows that $\kappa \sim M_w^{2n}$. Unlike bending rigidity, membrane viscosity shows more complex dependence on $M_w$. This finding opens new questions to explore in the future.

In summary, we demonstrate that the field-driven giant vesicle elongation can serve as a facile method to measure the viscosity of a variety of lipid and polymer bilayer membranes. The method is sensitive to variations in the degree of unsaturation in the carbon chain of lipids in single-component lipid membranes, composition and phase state in multi-component membranes and molecular weight dependence on polymersomes. The ease of implementation, high-throughput, minimal experimental equipment and effort as well as robustness make this technique suitable for every lab. Additional advantage is that not only viscosity but also membrane bending rigidity and tension can be simultaneously measured in one experiment (see supplemental material for details). We envision that this approach will become a standard tool for membrane characterization in every membrane biophysics and soft matter lab.

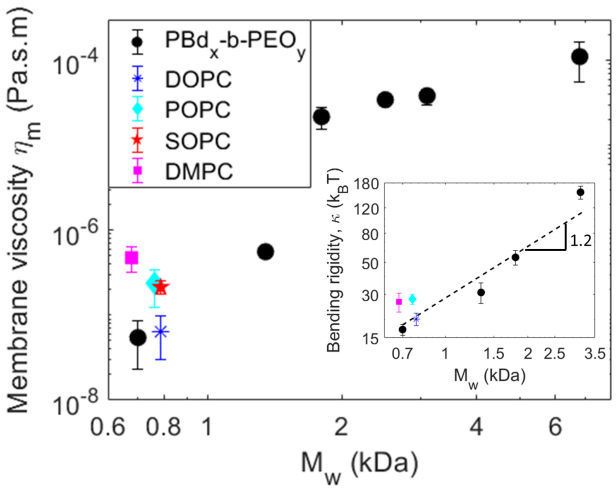


FIG. 4. Membrane viscosity of $PBd_x$-*b*-$PEO_y$ polymer GUVs. Here the membrane viscosity is varied with $M_w$. The viscosity of phospholipids are also plotted for comparison. The inset shows the bending rigidity of $PBd_x$-*b*-$PEO_y$ and phospholipids as a function of molecular weight.

TABLE III. Measured membrane viscosities for different polymerosomes with varying $M_w$ at temperature, 25.0 °C. The values in brackets indicate the number of measured vesicles per composition.

| Polymer | $M_w$ [kDa] | $\eta_m$ [$10^{-7}$ Pa.s.m] |
|---|---|---|
| $PBd_{13}$-*b*-$PEO_{11}$ | 0.70 | 0.55 ±0.31 (20) |
| $PBd_{22}$-*b*-$PEO_{14}$ | 1.35 | 5.57 ±0.70 (24) |
| $PBd_{33}$-*b*-$PEO_{20}$ | 1.85 | 216 ±64 (20) |
| $PBd_{46}$-*b*-$PEO_{24}$ | 2.60 | 342±47 (10) |
| $PBd_{54}$-*b*-$PEO_{29}$ | 3.10 | 381± 80 (10) |
| $PBd_{120}$-*b*-$PEO_{78}$ | 6.80 | 1100± 545 (10) |

PV and HF acknowledge financial support by NIH NIGMS award 1R01GM140461.

## Materials and Methods

### Vesicle Preparation

Giant unilamellar vesicles (GUVs) are formed from lipids and polymer such as palmitoyloleoylphosphatidylcholine (POPC), dioleoylphosphatidylcholine (DOPC), cholesterol (Chol), dimyristoylphosphatidylcholine (DMPC), stearoyloleoylphosphatdylcholine (SOPC), dipalmitoylphosphatidylcholine (DPPC) and poly(butadiene)-*b*-poly(ethylene oxide) diblock copolymers, $PBd_x$-*b*-$PEO_y$. The lipids and diblock copolymer were purchased from Avanti Polar Lipids (Alabaster, AL) and Polymer Source Inc. (Montreal, Canada), respectively. The multi-component vesicles made of DOPC/DPPC/Chol were fluorescently marked with 0.1 mol% of Liss Rhod PE. The lipid vesicles were produced using the electroformation method [41]. The stock solutions of 12 mM lipid in choloroform are diluted to 5 mM from which 10 $\mu$l of the solution is spread on the conductive sides of the ITO slides (Delta technologies, USA). The slides are stored in vacuum for 2-4 hours to evaporate all the organic solvents. The two slides are then sandwiched with a 2 mm thick teflon spacer and the electroformation chamber is filled with 40 mM sucrose solution in 0.5-1 mM of NaCl. The chamber is connected to a signal generator (Agilent, USA) for 2 hours at 50 Hz and voltage 1.5 V at $60^o$ C, which ensures that all lipids are above their main phase transition temperatures. The harvested vesicles are diluted in isotonic glucose solution in 1 mM NaCl. 3 independent GUV batches for every lipid composition were analyzed. Polymer vesicles were produced from spontaneous swelling method. Initially, 50 $\mu$l of 6-10 mg/ml (in chloroform) polymer solution was dissolved in 200-300 $\mu$l of chloroform in a 20 ml vial. Polymer films were formed from evaporation by blowing with a nitrogen stream while swirling the solution inside. Afterwards, the vials were dried under vacuum for 2-4 hours. The polymer films were hydrated in the suspending solutions (40 mM sucrose solution in 0.5-1 mM NaCl) and placed at 60 °C in an oven for 18-24 hours.

### Electrodeformation

The electrodeformation experiments are conducted in the electrofusion chamber (Eppendorf, Germany). The chamber is made from Teflon with two 92 $\mu$m cylindrical parallel electrodes 500 $\mu$m apart. The field is applied using a function generator (Agilent 3320A, USA). The function generator is controlled using a custom built MATLAB (Mathworks, USA) progam. This gives a precise control over the strength and duration of applied electric fields.

### Optical Microscopy and Imaging

The vesicles are visualized using a phase contrast microscope (A1 Axio Observer, Zeiss, Germany) with 63x objective 0.75 NA (air). High speed imaging is performed using Photron SA1.1 high speed camera. The image acquisition rate for electrodeformation recordings is kept to a constant of 500-2000 fps for lipid vesicles and 60-200 fps for polymer vesicles and the shutter speed is fixed to 500 $\mu$s. The time evolution of the vesicle is analyzed using a home-made image analysis software. The software uses a Fourier series to fit around the vesicle contour, $r_s = \sum_{n=0}^{\infty} \alpha_n \cos(n\theta) + \beta_n \sin(n\theta)$. The second mode in the series is used to determine the major ($a$) and minor axis ($b$) of the deformed vesicles to evaluate $\nu = \frac{a}{b} = \frac{1+\alpha_2}{1-\alpha_2}$.

The confocal imaging was performed with Leica TCS SP8 scanning confocal microscope using a HC PL APO 40x/ NA 1.3 (oil) objective. The pinhole size during the experiment was fixed to 1 AU (Airy units). The dye was excited with a 561 nm laser (diode-pumped solid-state laser) with 1.61% (laser intensity) HyD3 detector (hybrid).

### Equilibrium Fluctuation Analysis

Flickering spectroscopy is a popular technique to extract out membrane rigidity and tension due to its non-intrusive nature and well developed statistical analysis criteria. The details of the technique are given in [15, 27, 28]. Essentially, a time series of fluctuating vesicle contours is recorded on the focal plane. The quasi-circular contour is represented in Fourier modes, $r(\phi) = R\left(1 + \sum_q u_q(t) \exp(\mathrm{i}q\phi)\right)$. The fluctuating amplitudes $u_q$ have mean square amplitude dependence on the membrane bending rigidity $\kappa$ and the tension $\sigma$, $\langle |u_q|^2 \rangle \sim \frac{k_B T}{\kappa(q^3 + \bar{\sigma} q)}$, where $k_B T$ is the thermal energy ($k_B$ is the Boltzmann constant and T is the temperature), and $\bar{\sigma} = \sigma R^2/\kappa$. The fluctuations were recorded with phase contrast microscope (Axio Observer A1 Zeiss, Germany) using a 63x/ Numerical Aperture (NA) 0.75 Ph2

(air) objective at 60 fps with high speed camera (Photron SA1.1). The Focal depth, $FD$, was determined using the standard formula $d = \frac{l}{NA^2}$ where the wavelength, $l$, of transmission light is 550 nm. This results in FD= 0.97 $\mu m$ with the non dimensionalized $\Delta = \frac{FD}{R}$ (vesicle size range of radius, $R$, 20-50 $\mu m$) smaller than 0.05 to avoid the averaging effect of out of focus optical projections on equatorial projections [28]. The integration time effect of the camera was reduced by acquiring images at a low shutter speed of 100-200 $\mu$s. At least 5000 images were obtained for each vesicle for good statistics.

## Additional data

### Pure phospholipid or polymer system

TABLE IV. Measured membrane viscosities for different single-component bilayers (the number of measured vesicles is given in the brackets) compared with literature values.

| Composition | Area per lipid head [$\AA^2$] | Molecular weight $M_w$ [kDa] | Measured viscosity $\eta_m$ [$10^{-8}$ Pa.s.m] | Reference $\eta_m$[$10^{-8}$ Pa.s.m] |
|---|---|---|---|---|
| DOPC (18:1) | 67.4-75.4 [42–47] | 0.786 | 6.4 ±3.4 (19) | 0.01-2 [34, 48–54] |
| POPC (16:0-18:1) | 68.3 [55] | 0.760 | 23.4 ±11.1 (21) | 0.1-30000 [31, 52] |
| SOPC (18:0-18:1) | 67 [56] | 0.788 | 21.4 ±4.0 (20) | 170 [11] |
| DMPC (14:0) | 59.7-60.5 [57, 58] | 0.680 | 48.0 ±15.8 (17) | 0.05-50 [30, 53, 59] |
| $PBd_{22}$-*b*-$PEO_{14}$ | NA | 1.35 | 55.7 ±7.0 (22) | NA |

### DOPC-DPPC-Chol mixture

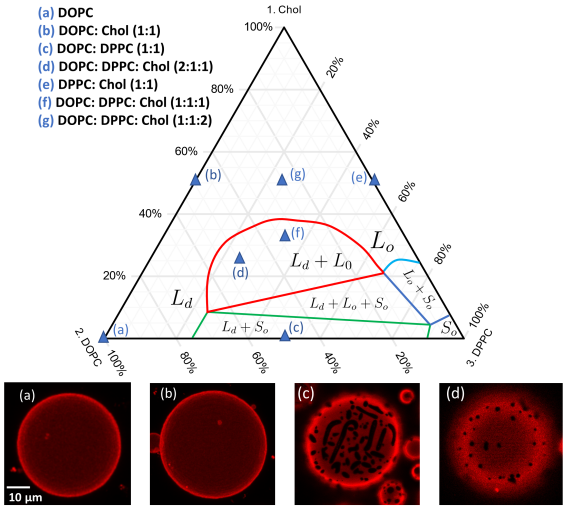


FIG. 5. DOPC:DPPC:Chol ternary system at temperature 25.0 $^o$C. Different letters represent the different compositions measured. Confocal microscopy images of vesicles with the following compositions (a) DOPC, (b) DOPC:Chol (1:1), (c) DOPC:DPPC (1:1), (d) DOPC:Chol:DPPC (2:1:1). The phase diagram is adapted and redrawn from *Uppamoochikkal et al.* [60] and the respective regions of liquid ordered $L_o$, liquid disordered $L_d$ and solid $S_o$ phase coexistence are indicated.

The different compositions investigated are indicated on Fig. 5. We have compared our results to the diffusion constants measured in this ternary system by *Scherfeld et al.* [35]. In general, increasing viscosity correlates with decreasing diffusivity as seen in Fig. 6, however, it is not trivial to directly compare the values of the diffusion constant and membrane viscosity as the former characterization is probe-dependent. For this reason, we compare the trends in both studies. The lipid mobility was reduced with the addition of cholesterol as the lipid ordering increases due to

TABLE V. Measured membrane viscosities for DOPC/DPPC/Chol ternary system at 25.0 $^o$C. The number of measured vesicles is given in the brackets. The diffusion constants measured by *Scherfeld et al.* [35] are listed for comparison.

| Composition | Measured viscosity $\eta_m[10^{-8}$ Pa.s.m] | Diffusion coefficient [35] $D[10^{-8}$ cm$^2$/s] |
|---|---|---|
| DOPC | 6.4 ±3.4 (19) | 6.30±0.13 |
| DOPC: Chol (1:1) | 20.5 ±13.0 (25) | 3.25±0.25 |
| DPPC:Chol (1:1) | 32.3 ±12.4 (25) | 0.48±0.06 |
| DOPC:DPPC (1:1) | 15.3 ±6.5 (20) | 5.90±0.30 |
| DOPC:DPPC:Chol (1:1:1) | 12.6 ±4.6 (18) | 2.50±0.20 |
| DOPC:DPPC:Chol (1:1:2) | 20.7 ±12.6 (25) | 1.85±0.13 |
| DOPC:DPPC:Chol (2:1:1) | 22.0 ±13.0 (22) | Not Available |

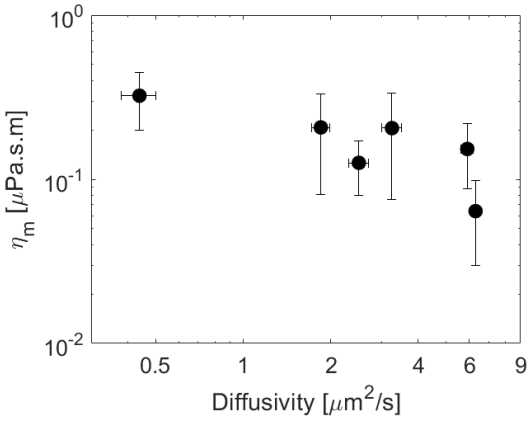


FIG. 6. Membrane viscosity obtained from this study as a function diffusivity values from *Scherfeld et al.* [35] for different membrane compositions as shown in Fig. 5.

tighter packing from Chol as shown from the DOPC:Chol (1:1) data in this study and ref. [35]. At 33 % cholesterol, DOPC:DPPC:Chol (1:1:1), the membrane fluidity was characterized by $\eta_m = 12.6 \pm 4.6 \times 10^{-8}$ Pa.s.m while the diffusion constant measured by *Scherfeld et al.* also showed a decreased lipid mobility $D = 2.5 \pm 0.2 \times 10^{-8}$ cm$^2$/s. At 50 % cholesterol, DOPC:DPPC:Chol (1:1:2), the lipid dynamics further slowed down $\eta_m = 20.7 \pm 12.6 \times 10^{-8}$ Pa.s.m suggesting an increase in the liquid ordering resulting from additional cholesterol confirmed by *Scherfeld et al.* with $D = 1.85 \pm 0.13 \times 10^{-8}$ cm$^2$/s.

## Vesicle deformation in an AC field

### Theory

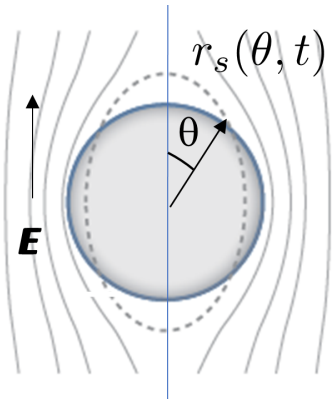

Upon application of a uniform electric field, an initially spherical vesicle deforms into an axisymmetric ellipsoid described by

$$r_s(\theta) = R\left(1 + s\left(3\cos^2\theta - 1\right)\right), \tag{3}$$

where $r_s$ is the position of the surface, $\theta$ is the angle with the applied field direction, $R$ is the radius of the vesicle and $s$ is the deformation parameter. The ellipsoid aspect ratio, defined as the ratio of the long and short axes, is $\nu \approx 1 + 3s$. The theory developed by *Vlahovska et al.* [17, 19–22] predicts that the deformation parameter, when deformations are small $s \ll 1$, evolves as

$$s(t) = \frac{p}{24\tilde{\sigma}}\left(1 - \exp\left(-t\frac{24\left(\tilde{\sigma} + 6\tilde{\kappa}\right)}{\eta(32 + 23\chi + 16\chi_m)}\right)\right) \tag{4}$$

where $\chi = \eta_{\rm v}/\eta$ is the ratio of the viscosities of the fluid inside and outside the vesicle (typically this parameter is 1, since the fluids are the same), $\chi_m = \eta_m/\eta R$ is the scaled membrane viscosity $\eta_m$, and $\tilde{\sigma} = \sigma/R$ and $\tilde{\kappa} = \kappa/R^3$ are the scaled tension and bending rigidity. $p$ is the electric stress exerted on the vesicle surface. In an AC electric field, $E = E_0\cos(\omega t)$,

$$p = \varepsilon E_0^2\left(2(1 - P_{\rm w}^r) + \frac{1}{2}P_{\rm w}^2 - 2SP_{\rm v}^2\right) \equiv \varepsilon E_0^2\hat{p} \tag{5}$$

where

$$\begin{aligned} P_{\rm w} &= \frac{K_{\rm w} + K_{\rm v}(V_m - 1)}{K_{\rm v} + 2K_{\rm w}}, \quad P_{\rm v} = \frac{K_{\rm w}(3 - 2V_m)}{K_{\rm v} + 2K_{\rm w}}, \\ V_m &= \frac{3K_{\rm v}K_{\rm w}}{2K_{\rm v}K_{\rm w} + {\rm i}C_m\left(K_{\rm v} + 2K_{\rm w}\right)\bar{\omega}} \end{aligned} \tag{6}$$

Here $\bar{\omega} = \omega\varepsilon/\sigma$, $K_{\rm v} = 1 + {\rm i}\bar{\omega}$ and $K_{\rm w} = \Lambda + {\rm i}\bar{\omega}S$ are the dimensionless complex permittivities. $S = \varepsilon_{\rm v}/\varepsilon$ and $\Lambda = \sigma_{\rm v}/\sigma$ are the ratios of permittivities and conductivities of the fluids interior and exterior to the vesicle. $P^r$ denotes the real part of $P$, and $P^2 = PP^*$.

Eq. 4 shows that if the membrane bending rigidity and tension, and the solution viscosities are known, measuring the vesicle deformation at given applied stress $p$ can yield the membrane viscosity. In this paper, we develop the method when $p$ is due to an applied uniform AC electric field. However, Eq. 4 applies to any ellipsoidal deformation of a vesicle, for example, driven by an applied extensional flow [61–63] or an optical trap [64]. In the case of applied flow, the traction $p$ can be found in [20, 22].

### Electrodeformation method to measure bending rigidity

The steady deformation of GUVs in AC uniform electric field has been proposed by Kummrow and Helfrich [14] as a method to determine the bending rigidity, since the increase in the apparent area associated with the deformation from a sphere to ellipsoid arises from ironing of suboptical shape undulations.

The increase in apparent area can be expressed as

$$\alpha(\nu) \equiv \frac{A(\sigma) - A(\sigma_0)}{A(\sigma_0)} = \frac{8}{45}\left(\nu - 1\right)^2, \tag{7}$$

assuming a quasi–spherical vesicle $A(\sigma_0) = 4\pi R^2$. In the entropic regime

$$\frac{A(\sigma) - A(\sigma_0)}{A(\sigma_0)} = \frac{k_BT}{8\pi\kappa}\log\left(\frac{\sigma}{\sigma_0}\right) \tag{8}$$

hence

$$\frac{k_BT}{4\kappa}\log\left(\frac{\sigma}{\sigma_0}\right) = 2\pi\alpha(\nu) \tag{9}$$

$\sigma(\nu)$ we get from the steady state deformation, $t \to \infty$ (see Eq. 4)

$$\sigma(\nu) = \frac{p}{8(\nu - 1)}, \tag{10}$$

Substituting in Eq. 9 yields

$$\frac{k_B T}{4\kappa} \log\left(\frac{\varepsilon E_0^2 R}{\sigma_0} \frac{\hat{p}}{8(\nu-1)}\right) = \frac{16\pi}{45}(\nu-1)^2 \tag{11}$$

Thus

$$\frac{k_B T}{4\kappa} \log\left(\frac{\varepsilon R \hat{p}}{8\sigma_0}\right) + \frac{k_B T}{4\kappa} \log\left(\frac{E_0^2}{\nu-1}\right) = \frac{16\pi}{45}(\nu-1)^2 \ . \tag{12}$$

To determine the bending rigidity, we measure the steady state aspect ratio $\nu$ at several applied electric field amplitudes (as in Fig. 2 in the main text) and utilize Eq. 12 to determine bending rigidity from the slope of the plot (note that the first term is constant for all field strengths). Details of the method is given in [15]. Taking the values from Fig. 2 in the main text yields for the bending rigidity of POPC $\kappa = 17.5\, k_B T$ which is consistent with the literature value [65].

### Sensitivity of the electrodeformation method to measure membrane viscosity

Our method relies on the equation

$$\nu(t) = 1 + \frac{9\varepsilon E_0^2 R}{64\sigma}\left(1 - \exp\left(-\frac{24\sigma}{\eta R\,(55+16\chi_m)}t\right)\right) \tag{13}$$

The linear approximation is only valid if the argument of the exponential function is

$$\frac{24\sigma t}{\eta R\,(55+16\chi_m)} \ll 1$$

The Taylor series of the exponential function is

$$\exp(-ct) = 1 - ct + \frac{(ct)^2}{2} + h.o.t.$$

$$\text{where for Eq. 13} \quad c = \frac{24\sigma}{\eta R\,(55+16\chi_m)}$$

It shows that the quadratic correction becomes comparable to the linear term when

$$ct = \frac{(ct)^2}{2} \Longrightarrow t = \frac{c}{2}$$

which gives the estimate for the time up to which the linear approximation is reasonable

$$\frac{t}{t_{\text{ed}}} = \frac{\varepsilon E_0^2 R\,(55+16\chi_m)}{12\sigma}$$

### Vesicle deformation and reproducibility

Fig. 7 illustrates a typical POPC vesicle deformation and the theoretical fitting with main text Eq. 2 to extract out membrane viscosity after several trials. In the particular example, a $R = 25.1$ $\mu$m vesicle is transiently electrodeformed multiple times at 8 kV/m. The results show high reproducibility of the initial slope after multiple electrodeformation pointing out the same membrane viscosity 2.0 $\pm 0.1 \times 10^{-7}$ Pa.s.m.

### Droplet electrodeformation

The electrodeformation method we have developed can be also applied to measure interfacial properties (interfacial tension and viscosity) of fluid droplets. Here, we show a proof of concept that the early stage of deformation dynamics of droplets, which have no interfacial viscosity, under electric field is governed by viscous dissipation in the bulk of the fluids and surface tension between fluids. The method can be extended to analyze interfacially-viscous droplets such as surfactant- or protein-laden, and nanoparticle-coated drops.

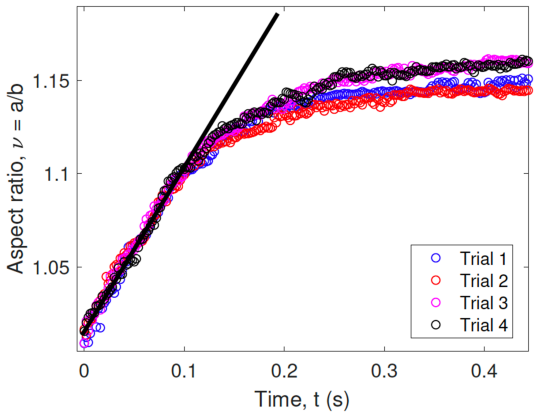


FIG. 7. GUV electrodeformation of a $R = 25.1$ *um* vesicle under the application of 8 kV/m electric field strength. The conditions are 0.5 mM NaCl in 40 mM Sucrose inside and 1 mM NaCl in 42 mM Glucose outside. The solid black line represents the theoretical fit for the data with main text Eq. 2.

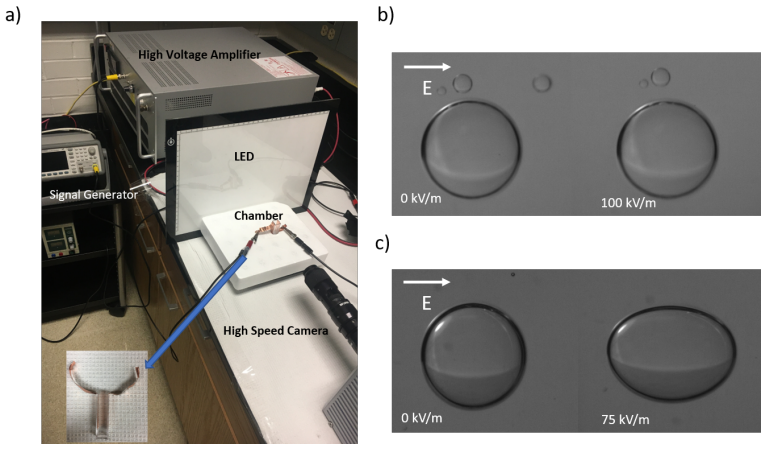


FIG. 8. a) The experimental setup b) Deformation of $R = 2$ mm size water droplet in castor oil without any surfactants c) Deformation of $R = 2$ mm size water droplet in castor oil with 0.5 % Tween 80.

### Experimental set-up

The experimental section for droplet deformation is shown in Fig. 8a. A rectangular acrylic cuvette (12 mm x 75 mm x 12 mm) is used as a chamber. Two copper electrodes are attached on the opposite sides of the cuvette. The electrodes are attached to a high voltage amplifier and signal generator (Agilent). A drop of water of radius 1-2 mm is dispensed into the chamber filled with castor oil using a micropipette (Eppendorf, USA). The droplet deformation is recorded using the high speed camera (Photron SA1, USA) and the image processing is performed in Matlab (Mathworks, USA). The setup was illuminated with back LED light source.

### Fluids for droplet deformation

Water (HPLC grade, Sigma Aldrich) and Castor oil (Sigma Aldrich) were used to form water in oil droplets. The properties of fluids are given in *Vizika et al.* [66] and summarized in Table VI. The interfacial tension of the droplets was modified with surfactants, Tween 80 (Sigma Aldrich) and Span 80 (Sigma Aldrich).

TABLE VI. Material properties of the fluids obtained from [66, 67]

| Material | Density kg/m$^3$ | Relative permittivity | Conductivity S/m | Viscosity Pa.s |
|---|---|---|---|---|
| Water | 997 | 78 | $1\times10^{-4}$ | $8.9\times10^{-4}$ |
| Castor Oil | 961 | 5.3 | $3.8\times10^{-11}$ | 0.69 |

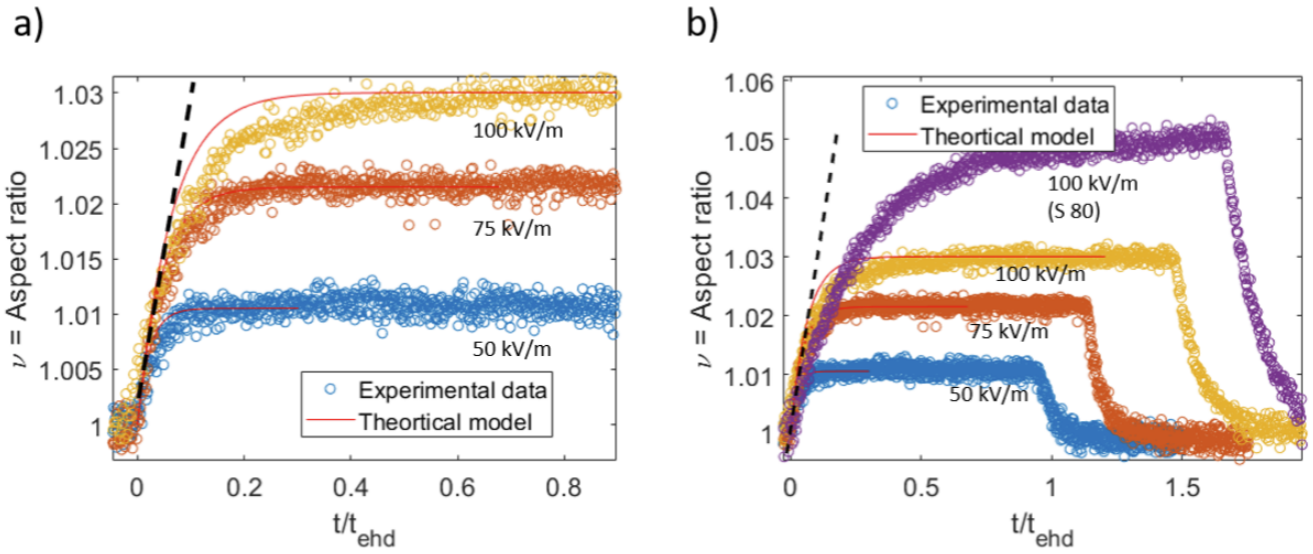


FIG. 9. a) Deformation of $R = 2$ mm size water droplet in castor oil without any surfactants. The red solid line is represented by Eq. 14 while black dashed line is given by Eq. 15 b) Deformation of $R = 2$ mm size water droplet in castor oil with 2 % Span 80.

**Results**

Let us consider a drop with radius $R$. The degree of deformation depends on the ratio between Maxwell electrical stress and $\varepsilon_w E_0^2$ and capillary stress $\sigma/R$, which defines the Capillary Number, $Ca = \frac{\varepsilon_w E_0^2 R}{\sigma}$. The deformation depends on the ratio of electrical permittivities, $S = \varepsilon_v/\varepsilon_w$, conductivities, $\Lambda = \sigma_v/\sigma_w$, and bulk viscosities $\chi = \eta_v/\eta_w$. The shape evolution of drop deformation in a uniform electric field is given by [20, 21, 68]:

$$\nu = \frac{9\,(5+6\Lambda+5\Lambda^2+\chi(5+9\Lambda+5\Lambda^2-19S)-16S)}{80\,(1+\chi)\,(2+\Lambda)^2}\,Ca\left[1-\exp\left(-\frac{40(1+\chi)}{Ca(3+2\chi)(16+19\chi)}\,\frac{t}{t_{ed}}\right)\right]+1 \tag{14}$$

Note time in non-dimensionalized by the electrohydrodynamic time scale $t_{ed} = \frac{\eta_w}{\varepsilon_r E_0^2}$. Here we have worked at low frequencies of 500 Hz for each experiment.

At short times, Eq. 14 simplifies to:

$$\nu = 1 + \frac{9\,(5+6\Lambda+5\Lambda^2+\chi(5+9\Lambda+5\Lambda^2-19S)-16S)}{2(3+2\chi)(16+19\chi)(2+\Lambda)^2}\,\frac{t}{t_{ed}} \tag{15}$$

It can be seen Eq. 15 is a linear equation in time only dependent on dissipation in bulk viscosity of the fluids and independent of surface tension. It determines the initial rate of deformation. This equation is similar to Eq. 2 in the main text for bilayer membranes. For a water droplet in castor oil of $R = 1$ mm with field strength of 100 kV/m $t_{ed} \sim 1s > t_\sigma \sim 0.1$ so Eq. 15 approximation can not be applied and one has to fit the whole curve with Eq. 14 as shown in Fig. 9a. In other words as soon as the electric field is turned on, membrane tension dictates shape evolution of droplets due to a much higher surface tension. Note here we have not used any fitting parameter. The surface tension is $12 \pm 2$ mN/m (based on 10 different droplets) which is slightly lower than reported values from *Vizika et al* [66] of 16.8 mN/m. We believe this could be due small impurities in fluids. Hence, in the case of simple interfaces like droplets, the approximation, to use initial deformation rate to determine viscosity ratio $\lambda$ cannot be used simply due to a large surface tension. Note GUVs have membrane tension ($\sim 10^{-8}$ N/m) much smaller than droplet surface tension ($\sim 10^{-3}$ N/m) hence the criteria meets well $t_{ed} < t_\sigma$.

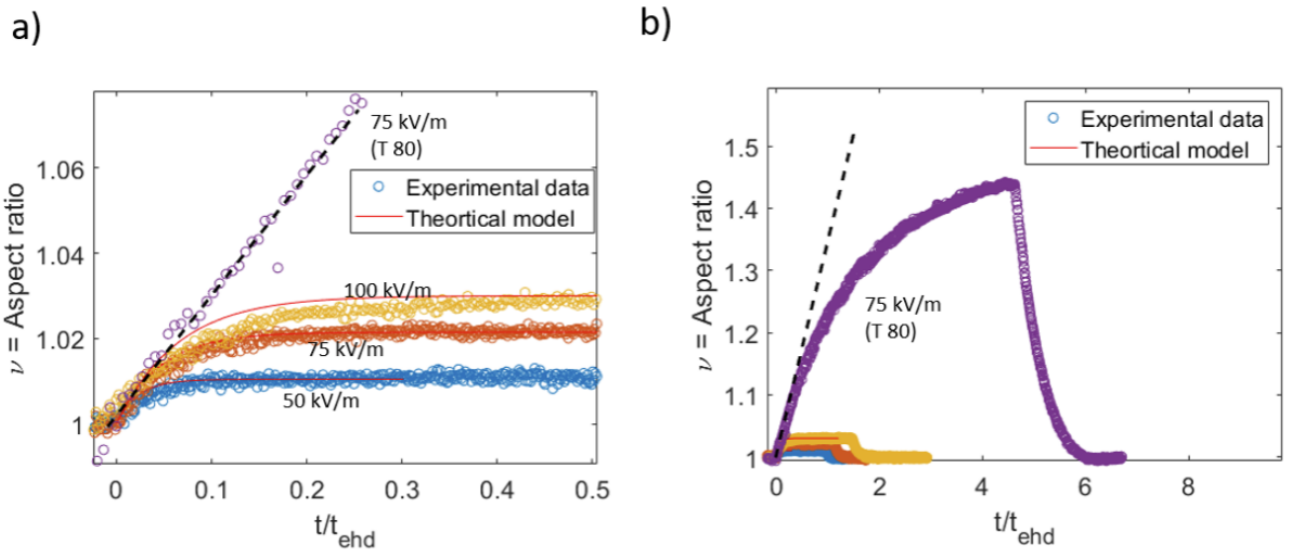


FIG. 10. a) Deformation of $R = 2$ mm size water droplet in castor oil with 0.5 % Tween 80. The red solid line is represented by Eq. 14 while black dashed line is given by Eq. 15 b) Same Fig. as part (a) but on a longer time scale

For water in castor oil system, there are three ways to meet the above criteria: increase the field strength, add surfactants to lower the surface tension or deform much larger size droplets. The larger size droplets idea cannot be used simply due the effects of sedimentation that would create additional flows. We cannot meet the first criteria either due to highest field strength provided by the high voltage amplifier (100 kV/m for a 1 cm size cuvette). To meet the surface tension criteria, we added 2.0% (w/w) Span 80 (S 80) and 0.5% (w/w) Tween 80 (T 80) as surfactants (see Fig. 9b and Fig. 10a b). We found out that the surface tension was lowered by approximately 20 times for the Tween 80 case. This leads to $t_{\rm ed} \sim t_\sigma$ and the approximation improved, see 10a b). However, even after lowering the surface tension by 20 times Eq. 15 cannot be solely used with good sensitivity because of the similar time scale.


[1] S. J. Singer and G. L. Nicolson, Science **175**, 720 (1972).
[2] A. E. Cohen and Z. Shi, BioEssays **42**, 1900142 (2020).
[3] R. Illukkumbura, T. Bland, and N. W. Goehring, Current Opinion in Cell Biology **62**, 123 (2020).
[4] P. Cicuta, S. L. Keller, and S. L. Veatch, The Journal of Physical Chemistry B **111**, 3328 (2007).
[5] E. P. Petrov, R. Petrosyan, and P. Schwille, Soft Matter **8**, 7552 (2012).
[6] S. Block, Biomolecules **8** (2018).
[7] T. T. Hormel, S. Q. Kurihara, M. K. Brennan, M. C. Wozniak, and R. Parthasarathy, Phys. Rev. Lett. **112**, 188101 (2014).
[8] B. A. Camley, C. Esposito, T. Baumgart, and F. L. Brown, Biophysical Journal **99**, L44 (2010).
[9] M. Nagao, E. G. Kelley, R. Ashkar, R. Bradbury, and P. D. Butler, The Journal of Physical Chemistry Letters **8**, 4679 (2017).
[10] M. K. Kuimova, Phys. Chem. Chem. Phys. **14**, 12671 (2012).
[11] R. Waugh, Biophysical Journal **38**, 29 (1982).
[12] A. R. Honerkamp-Smith, F. G. Woodhouse, V. Kantsler, and R. E. Goldstein, Phys. Rev. Lett. **111**, 038103 (2013).
[13] Y. Sakuma, T. Kawakatsu, T. Taniguchi, and M. Imai, Biophysical Journal **118**, 1576 (2020).
[14] M. Kummrow and W. Helfrich, Phys. Rev. A **44**, 8356 (1991).
[15] R. S. Gracia, N. Bezlyepkina, R. L. Knorr, R. Lipowsky, and R. Dimova, Soft Matter **6**, 1472 (2010).
[16] M. Yu, R. B. Lira, K. A. Riske, R. Dimova, and H. Lin, Phys. Rev. Lett. **115**, 128303 (2015).
[17] P. M. Vlahovska, in *Advances in Planar Lipid Bilayers and Liposomes, vol. 12*, edited by A. Iglic (Elsevier, 2010) pp. 103–146.
[18] P. F. Salipante and P. M. Vlahovska, Soft Matter **10**, 3386 (2014).
[19] P. M. Vlahovska, R. S. Gracia, S. Aranda-Espinoza, and R. Dimova, Biophys. J. **96**, 4789 (2009).
[20] P. M. Vlahovska, in *Low-Reynolds-Number Flows: Fluid-Structure Interactions*, edited by C. Duprat and H. Stone (2016).
[21] P. M. Vlahovska, Annu. Rev. Fluid Mech. **51**, 305 (2019).
[22] P. M. Vlahovska and C. Misbah, in *The Giant Vesicle Book*, edited by R. Dimova and C. Marques (CRC Press, 2019) p. Chapter 7.
[23] T. Portet and R. Dimova, Biophysical Journal **99**, 3264 (2010).
[24] D. Needham and R. Hochmuth, Biophysical Journal **55**, 1001 (1989).
[25] H. Bermúdez, H. Aranda-Espinoza, D. A. Hammer, and D. E. Discher, EPL (Europhysics Letters) **64**, 550 (2003).

[26] H. Aranda-Espinoza, H. Bermudez, F. S. Bates, and D. E. Discher, Phys. Rev. Lett. **87**, 208301 (2001).

[27] H. A. Faizi, S. L. Frey, J. Steinkühler, R. Dimova, and P. M. Vlahovska, Soft Matter **15**, 6006 (2019).

[28] H. A. Faizi, C. J. Reeves, V. N. Georgiev, P. M. Vlahovska, and R. Dimova, Soft Matter **16**, 8996 (2020).

[29] R. Dimova, B. Pouligny, and C. Dietrich, Biophysical Journal **79**, 340 (2000).

[30] R. Dimova, C. Dietrich, A. Hadjiisky, K. Danov, and B. Pouligny, The European Physical Journal B - Condensed Matter and Complex Systems **12**, 589 (1999).

[31] G. Espinosa, I. López-Montero, F. Monroy, and D. Langevin, PNAS **108**, 6008 (2011).

[32] K. J. Seu, L. R. Cambrea, R. M. Everly, and J. S. Hovis, Biophysical Journal **91**, 3727 (2006).

[33] B. A. Camley and F. L. H. Brown, The Journal of Chemical Physics **151**, 124104 (2019).

[34] S. Chakraborty, M. Doktorova, T. R. Molugu, F. A. Heberle, H. L. Scott, B. Dzikovski, M. Nagao, L.-R. Stingaciu, R. F. Standaert, F. N. Barrera, J. Katsaras, G. Khelashvili, M. F. Brown, and R. Ashkar, PNAS **117**, 21896 (2020).

[35] D. Scherfeld, N. Kahya, and P. Schwille, Biophysical Journal **85**, 3758 (2003).

[36] C. F. Brooks, G. G. Fuller, C. W. Frank, and C. R. Robertson, Langmuir **15**, 2450 (1999).

[37] R. Dimova, U. Seifert, B. Pouligny, S. Förster, and H.-G. Döbereiner, The European Physical Journal E **7**, 241 (2002).

[38] G. Battaglia and A. J. Ryan, Journal of the American Chemical Society **127**, 8757 (2005).

[39] G. Srinivas, D. E. Discher, and M. L. Klein, Nature Materials **3**, 638 (2004).

[40] H. Bermúdez, D. A. Hammer, and D. E. Discher, Langmuir **20**, 540 (2004).

[41] M. I. Angelova and D. S. Dimitrov, Faraday Discuss. Chem. Soc. **81**, 303 (1986).

[42] S. Tristram-Nagle, H. I. Petrache, and J. F. Nagle, Biophysical Journal **75**, 917 (1998).

[43] J. F. Nagle and S. Tristram-Nagle, Biochimica et Biophysica Acta (BBA) - Reviews on Biomembranes **1469**, 159 (2000).

[44] Y. Liu and J. F. Nagle, Phys. Rev. E **69**, 040901 (2004).

[45] N. Kucerka, S. Tristram-Nagle, and J. F. Nagle, The Journal of Membrane Biology **208**, 193 (2006).

[46] N. Kučerka, J. F. Nagle, J. N. Sachs, S. E. Feller, J. Pencer, A. Jackson, and J. Katsaras, Biophysical Journal **95**, 2356 (2008).

[47] J. Pan, T. T. Mills, S. Tristram-Nagle, and J. F. Nagle, Phys. Rev. Lett. **100**, 198103 (2008).

[48] A. R. Honerkamp-Smith, B. B. Machta, and S. L. Keller, Phys. Rev. Lett. **108**, 265702 (2012).

[49] P. Cicuta, S. L. Keller, and S. L. Veatch, The Journal of Physical Chemistry B **111**, 3328 (2007).

[50] E. P. Petrov, R. Petrosyan, and P. Schwille, Soft Matter **8**, 7552 (2012).

[51] T. Hormel, M. Reyer, and R. Parthasarathy, Biophysical Journal **109**, 732 (2015).

[52] Y. Wu, M. Stefl, A. Olzynska, M. Hof, G. Yahioglu, P. Yip, D. R. Casey, O. Ces, J. Humpolíková, and M. K. Kuimova, Physical Chemistry Chemical Physics **15**, 14986 (2013).

[53] Y. Nojima and K. Iwata, The Journal of Physical Chemistry B **118**, 8631 (2014), pMID: 24967901, https://doi.org/10.1021/jp503921e.

[54] W. L. C. Vaz, M. Criado, V. M. C. Madeira, G. Schoellmann, and T. M. Jovin, Biochemistry **21**, 5608 (1982), pMID: 6216914, https://doi.org/10.1021/bi00265a034.

[55] N. Kučerka, S. Tristram-Nagle, and J. F. Nagle, The Journal of Membrane Biology **208**, 193 (2006).

[56] A. I. Greenwood, J. Pan, T. T. Mills, J. F. Nagle, R. M. Epand, and S. Tristram-Nagle, Biochimica et Biophysica Acta (BBA) - Biomembranes **1778**, 1120 (2008).

[57] H. I. Petrache, S. Tristram-Nagle, and J. F. Nagle, Chemistry and Physics of Lipids **95**, 83 (1998).

[58] N. Kučerka, Y. Liu, N. Chu, H. I. Petrache, S. Tristram-Nagle, and J. F. Nagle, Biophysical Journal **88**, 2626 (2005).

[59] W. den Otter and S. Shkulipa, Biophysical Journal **93**, 423 (2007).

[60] P. Uppamoochikkal, S. Tristram-Nagle, and J. F. Nagle, Langmuir **26**, 17363 (2010).

[61] L. Guillou, J. Dahl, J.-M. Lin, A. Barakat, J. Husson, S. Muller, and S. Kumar, Biophysical Journal **111**, 2039 (2016).

[62] A. Shenoy, C. V. Rao, and C. M. Schroeder, PNAS **113**, 3976 (2016).

[63] D. Kumar, C. M. Richter, and C. M. Schroeder, Soft Matter **16**, 337 (2020).

[64] S.-H. Wu, S. Sankhagowit, R. Biswas, S. Wu, M. L. Povinelli, and N. Malmstadt, Soft Matter **11**, 7385 (2015).

[65] R. Dimova, Advances in Colloid and Interface Science **208**, 225 (2014), special issue in honour of Wolfgang Helfrich.

[66] O. Vizika and D. A. Saville, J. Fluid Mech. **239**, 1 (1992).

[67] P. F. Salipante and P. M. Vlahovska, Physics of Fluids **22**, 112110 (2010), https://doi.org/10.1063/1.3507919.

[68] J. T. Schwalbe, F. R. Phelan, P. M. Vlahovska, and S. D. Hudson, Soft Matter **7**, 7797 (2011).